Femtosecond Transfer and Manipulation of Persistent Hot-Trion Coherence in a Single CdSe/ZnSe Quantum Dot

P. Henzler,[1] C. Traum,[1] M. Holtkemper,[2] D. Nabben,[1] M. Erbe,[1] D. E. Reiter,[2] T. Kuhn,[2] S. Mahapatra,[3,*] K. Brunner,[3] D. V. Seletskiy,[1,4] and A. Leitenstorfer[1,†]

[1]*Department of Physics and Center for Applied Photonics, University of Konstanz, D-78457 Konstanz, Germany*
[2]*Institute of Solid State Theory, University of Münster, D-48149 Münster, Germany*
[3]*Institute of Physics, EP3, University of Würzburg, D-97074 Würzburg, Germany*
[4]*Department of Engineering Physics, Polytechnique Montréal, Montréal, Québec H3T 1J4, Canada*

(Received 10 July 2020; accepted 7 December 2020; published 9 February 2021; corrected 14 April 2021)

Ultrafast transmission changes around the fundamental trion resonance are studied after exciting a *p*-shell exciton in a negatively charged II-VI quantum dot. The biexcitonic induced absorption reveals quantum beats between hot-trion states at 133 GHz. While interband dephasing is dominated by relaxation of the *P*-shell hole within 390 fs, trionic coherence remains stored in the spin system for 85 ps due to Pauli blocking of the triplet electron. The complex spectrotemporal evolution of transmission is explained analytically by solving the Maxwell-Liouville equations. Pump and probe polarizations provide full control over amplitude and phase of the quantum beats.

DOI: 10.1103/PhysRevLett.126.067402

Technological advances based on genuine quantum phenomena combine multiple opportunities and challenges. In general, the coherence time is a crucial parameter [1,2]. Therefore, understanding intrinsic relaxation and dephasing mechanisms in elementary quantum systems is key to further progress [3–5]. Long-lived coherences are typically assigned to electronic states close to equilibrium, where protection from pure dephasing is well known [6–10]. Despite the importance of highly excited states for quantum technology [11,12], their relaxation and dephasing dynamics remains poorly understood. In this context, the restricted phase space and large transition dipoles in semiconductor quantum dots (QDs) [13] offer interesting perspectives for spin-to-photon interfaces [2,14–17]. Specimens based on II-VI compounds may be especially advantageous since strong electronic confinement and Coulomb interactions enhance energy separations [18], enabling coherent manipulation even with femtosecond light pulses [14]. In principle, driving such quantum systems far from equilibrium allows to study both lifetime and potential transfer of quantum coherence between excited states as well as full relaxation pathways of individual charge carriers.

In this Letter, we report ultrafast generation and manipulation of a persistent coherence between excited trion states of a single negatively charged CdSe/ZnSe QD. Spectral changes of induced absorption into biexcitonic states directly reveal quantum beats between trion triplet states. Very surprisingly, the coherence between hot-trion states is transferred upon scattering of the photoexcited hole within 390 fs. Subsequently, it remains protected by the Pauli blocking of hot-electron relaxation and persists for 85 ps, i.e., almost three orders of magnitude longer than the timescale required for coherently initializing and manipulating the quantum system.

Our experimental setup consists of a three-color femtosecond fiber source coupled to a polarization-sensitive transmission microscope operating at 1.6 K [19]. Individual CdSe/ZnSe QDs [20,21] are embedded into subwavelength Al apertures to increase light-matter coupling [14,19]. Interband excitation generates a trion comprising two electrons and one hole. Figure 1(a) shows a microphotoluminescence spectrum. At an energy of 2.1482 eV, the radiative recombination X^- of the trion ground state ($|TGS\rangle$) into the global ground state ($|QDGS\rangle$) is observed. Two emission lines XX_X^- and XX_Y^- appear redshifted to X^- at energies of 2.1429 and 2.1434 eV, respectively. A quadratic increase of intensity with excitation power [21] assigns them to recombination of the charged biexciton ground state ($|CBGS\rangle$) into trion triplet states $|X\rangle$ and $|Y\rangle$ [28], which are spectrally split by (550 ± 5) μeV. Note that we work with an excitation intensity weak enough to ensure a low probability for generation of a biexciton by the pump. A level scheme together with relevant electronic configurations is depicted in Fig. 1(b). $|X\rangle$ and $|Y\rangle$ are both composed of one hole in the *S* shell of the valence band and two electrons, one each in the conduction-band *s* and *p* shells. $|X^*\rangle$ and $|Y^*\rangle$ have identical electron configurations but the hole occupies the *P* shell. Various spin configurations split in energy by exchange interactions emerge [14,28–31]. Specifically, the electron-electron exchange lifts the degeneracy between singlet and triplet configurations. Electron-hole exchange then separates the triplet states into two bright levels $|X\rangle$ and $|Y\rangle$, depending on the in-plane asymmetry of the confinement potential. Close to cylindrical symmetry, XX_X^- and

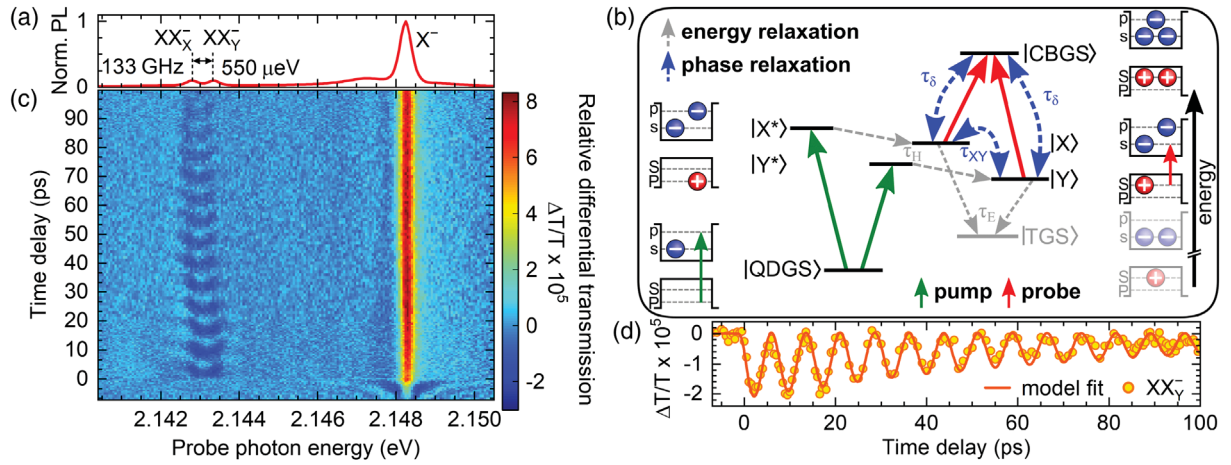

FIG. 1. Relative differential transmission of a single CdSe/ZnSe QD. Pulses polarized linearly along $\vec{e}_X - \vec{e}_Y$ initialize a superposition of excited states $|X^*\rangle$ and $|Y^*\rangle$, probed collinearly. (a) Microphotoluminescence. X^- denotes the fundamental trion resonance. XX_X^- and XX_Y^- indicate recombination of the biexciton ground state $|CBGS\rangle$ into triplet states $|X\rangle$ or $|Y\rangle$. (b) Few-level system. Radiative and nonradiative transitions are marked with solid (green and red for pumping and probing) and dashed gray arrows, respectively. Dashed blue arrows indicate phase relationships between eigenstates. τ_H marks the hole relaxation time, τ_E the p-shell electron relaxation time, τ_δ the interband dephasing time and τ_{XY} the dephasing time of the quantum beats. (c) Relative differential transmission $\Delta T/T$ color-coded versus photon energy and pump-probe delay time. (d) Dynamics of $\Delta T/T$ around XX_Y^-, visualized as yellow-orange circles with an error margin of $\pm 2 \times 10^{-6}$. The orange line represents a least-square fit to our theory.

XX_Y^- are circularly polarized. $|X\rangle$ and $|Y\rangle$ then decay into the $|TGS\rangle$ with distinctly different relaxation times [14]. A significant deviation from cylindrical symmetry results in a linear polarization of XX_X^- and XX_Y^- [28] along the principal axes $\vec{e}_X$ and $\vec{e}_Y$ of the confinement potential and similar relaxation rates of $|X\rangle$ and $|Y\rangle$, respectively. Polarization-sensitive photoluminescence (PL) spectroscopy assigns our QD to the latter type [21].

We now excite p-shell transitions of the QD initializing a coherent superposition of $|X^*\rangle$ and $|Y^*\rangle$ with 520-fs pulses of a central photon energy of 2.228 eV and spectral width of 5 meV, which are linearly polarized along $\vec{e}_X - \vec{e}_Y$ [green arrows in Fig. 1(b)]. 100-fs probe pulses are collinearly polarized and centered at 2.145 eV. Their bandwidth of 25 meV covers the entire range of fundamental trion and biexciton emission. Typical average powers for incident excitation and readout pulse trains are 10 and 1 μW, corresponding to pulse areas of 0.72π and 0.22π, respectively [21]. Figure 1(c) shows the color-coded relative differential transmission $\Delta T/T$ as a function of photon energy and time delay t_D between pumping and probing. Where probe pulses precede excitation at negative t_D, delay-dependent modulations at X^- result from a perturbed free induction decay [15,32]. For positive t_D, two processes contribute equally to the signal at X^-. First, ultrafast bleaching due to Coulomb renormalization [14,15] results in a steep increase to half of the maximum $\Delta T/T$ on a timescale below 1 ps [21]. Subsequently, single-photon gain emerges on a 100-ps timescale when population inversion between $|TGS\rangle$ and $|QDGS\rangle$ is established, directly revealing the intraband scattering times from $|X^*\rangle$ and $|Y^*\rangle$ into $|TGS\rangle$ [14]. As we will show below, the timescale for establishing the $|TGS\rangle$ is completely dominated by electron relaxation because the scattering of the hole, i.e., the step from $|X^*\rangle$ or $|Y^*\rangle$ to $|X\rangle$ or $|Y\rangle$, respectively, proceeds very rapidly. A $|TGS\rangle$ recombination time $\tau_{|TGS\rangle}$ of (366 ± 33) ps is deduced from $\Delta T/T$ at even longer delays. At the energy of XX_X^- and XX_Y^-, negative signatures appear for positive t_D. They originate from activating optical transitions from $|X\rangle$ and $|Y\rangle$ into $|CBGS\rangle$, as indicated by red arrows in Fig. 1(b). The most striking feature in this region is a long-lived periodic modulation of the line shape of biexcitonic induced absorption. A fast Fourier transform of $\Delta T/T$ at XX_Y^- reveals an oscillation frequency of (133 ± 2) GHz, coinciding exactly with the energy difference between the biexcitonic emission lines of (550 ± 5) μeV. This finding suggests that the signal emerges from quantum beats between $|X\rangle$ and $|Y\rangle$, as indicated by a dashed blue arrow and dephasing time τ_{XY} in Fig. 1(b). The modulation is analyzed in more detail in Fig. 1(d). The yellow-orange circles result from spectrally integrating $\Delta T/T$ around the position of XX_Y^- within an interval of 0.4 meV. The decay of the amplitude is caused by the relaxation of the p-shell electron to the s shell, corresponding to the transitions from $|X\rangle$ and $|Y\rangle$ into $|TGS\rangle$. From a model fit to the data in Fig. 1(d), we extract a time constant of $\tau_E = (85 \pm 10)$ ps for this process [see gray dashed arrows in Fig. 1(b)]. The consistency of our picture is underlined by the rise time of single-photon gain at X^- [Fig. 1(c)] of (83 ± 12) ps [21]: scattering of electrons from the p shell directly populates the s shell, thus establishing the $|TGS\rangle$ with a time constant identical to τ_E. Compared to other excited trion states [14], the lifetime of $|X\rangle$ and $|Y\rangle$ is 1–2 orders of magnitude

longer and merely a factor of five shorter than the interband recombination time $\tau_{|\mathrm{TGS}\rangle}$. These unusual conditions are due to Pauli blocking by the resident electron: relaxation of a triplet electron requires a combined electron-hole spin flip [14,30], rendering these states metastable. While energy relaxation is encoded in the signal envelope in Fig. 1(d), the trion coherence manifests itself in the contrast of the underlying oscillations. Interestingly, the quantum beats are clearly present and even persist over the entire temporal range of finite amplitude of biexcitonic absorption. This finding indicates that the coherence between $|\mathrm{X}^*\rangle$ and $|\mathrm{Y}^*\rangle$ is conserved during the relaxation into $|\mathrm{X}\rangle$ and $|\mathrm{Y}\rangle$ and even remains protected from pure dephasing: the decay time τ_{XY} of (85 ± 10) ps we extract from the oscillation contrast again coincides with τ_E. Obviously, the coherence is limited exclusively by the population relaxation of $|\mathrm{X}\rangle$ and $|\mathrm{Y}\rangle$, requiring a combined electron-hole spin flip. Note that τ_{XY} is much larger than the interband dephasing time τ_δ of (3.7 ± 0.5) ps between $|\mathrm{X}\rangle \leftrightarrow |\mathrm{CBGS}\rangle$ and $|\mathrm{Y}\rangle \leftrightarrow |\mathrm{CBGS}\rangle$ derived from the PL linewidth of $\mathrm{XX}^-_{\mathrm{X}}$ and $\mathrm{XX}^-_{\mathrm{Y}}$ of (360 ± 30) μeV which is not limited by our spectral resolution of 100 μeV [19].

Considering the carrier-phonon interaction within a Lindblad model provides a microscopic understanding of both the conservation of coherence during relaxation of the hole and the absence of pure dephasing thereafter [21,33,34]. The essential point is that the electron-phonon coupling acts solely on the orbital part of an electronic wave function. Both $|\mathrm{X}\rangle$ and $|\mathrm{Y}\rangle$ as well as $|\mathrm{X}^*\rangle$ and $|\mathrm{Y}^*\rangle$ share the same orbital state and only differ in their spin configuration. Thus, on the one hand, a pure relaxation of the orbital part of the hole from P to S shell does not affect the spin coherence between $|\mathrm{X}\rangle$ and $|\mathrm{Y}\rangle$ or $|\mathrm{X}^*\rangle$ and $|\mathrm{Y}^*\rangle$. On the other hand, all phonon scattering processes between coherent superpositions of $|\mathrm{X}\rangle$ and $|\mathrm{Y}\rangle$ or $|\mathrm{X}^*\rangle$ and $|\mathrm{Y}^*\rangle$ are strongly correlated, thus preventing pure dephasing.

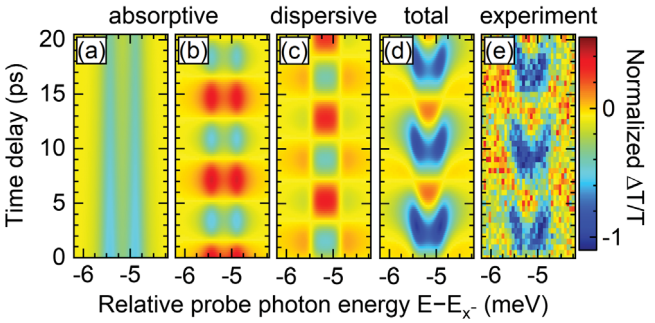

FIG. 2. Temporal evolution of analytical and experimental $\Delta T/T$ around the biexcitonic absorption color-coded versus photon energy relative to the X^- transition at 2.1482 eV. Calculated static-absorptive (a), modulated-absorptive (b), and dispersive contributions (c) add up to the total signal (d). The corresponding subset of experimental data from Fig. 1(c) is depicted in (e).

To analyze the lineshape modulation of biexcitonic signatures in Fig. 1(c), we calculate $\Delta T/T$ using the Maxwell-Liouville equations. The polarization of the QD acts as a source for a reemitted field which is superimposed with the much stronger probe field, forming the total transmitted electric field [35]. For an analytical solution, we restrict ourselves to linearly polarized transitions and assume $\delta(t)$-shaped pulses [21]. The result coincides with a numerical solution including realistic light pulses and states based on a configuration interaction approach [29]. Adopting small probe intensities and identical transition dipoles from $|\mathrm{QDGS}\rangle$ into $|\mathrm{X}^*\rangle$ and $|\mathrm{Y}^*\rangle$ as well as from $|\mathrm{X}\rangle$ and $|\mathrm{Y}\rangle$ into $|\mathrm{CBGS}\rangle$ [36,37], we find

$$(\Delta T/T)_{\mathrm{X/Y}} \sim \frac{-1/\tau_\delta}{1/\tau_\delta^2 + (\omega_{\mathrm{X/Y}} - \omega)^2} \cdot \left(\underbrace{e^{-t_D/\tau_E}}_{(A)} + \underbrace{e^{-t_D/\tau_{\mathrm{XY}}} \cos(\omega_{\mathrm{XY}} t_D + \vartheta)}_{(B)} \right) \mp \frac{\omega_{\mathrm{X/Y}} - \omega}{1/\tau_\delta^2 + (\omega_{\mathrm{X/Y}} - \omega)^2} \cdot \underbrace{e^{-t_D/\tau_{\mathrm{XY}}} \sin(\omega_{\mathrm{XY}} t_D + \vartheta)}_{(C)}, \tag{1}$$

where $\omega_{\mathrm{X/Y}}$ correspond to the photon frequencies of transitions $\mathrm{XX}^-_{\mathrm{X/Y}}$ and $\omega_{\mathrm{XY}} = \omega_{\mathrm{Y}} - \omega_{\mathrm{X}}$. As discussed below, the relative polarization of excitation and readout defines the phase ϑ of the oscillations. The total differential transmission is $\Delta T/T = (\Delta T/T)_{\mathrm{X}} + (\Delta T/T)_{\mathrm{Y}}$. Three major contributions evident from the right-hand side of Eq. (1) are visualized in Fig. 2.

The first part of the solution referring to term (A) in Eq. (1) is depicted in Fig. 2(a). It even occurs for an incoherent occupation of $|\mathrm{X}\rangle$ and $|\mathrm{Y}\rangle$ and is described by a Lorentzian-shaped absorption for each transition without any temporal modulation. The second (B) and third (C) parts of Eq. (1) are related to the excitonic coherence. Consequently, they oscillate with ω_{XY} and decay with $e^{-t_D/\tau_{\mathrm{XY}}}$. Part (B) is visualized in Fig. 2(b). It corresponds to a periodic modulation of the statically induced absorption in Fig. 2(a) with the beating frequency ω_{XY}. Interestingly, a third component (C) arises [see Fig. 2(c)], which is phase shifted by $\pi/2$ with respect to the direct modulation of absorption [Fig. 2(b)]: the nonstationary evolution of the electronic states causes a phase modulation of the reemitted field [21], creating new frequency components in regions of maximum temporal change. The full evolution of transient transmission is obtained by summing all three contributions

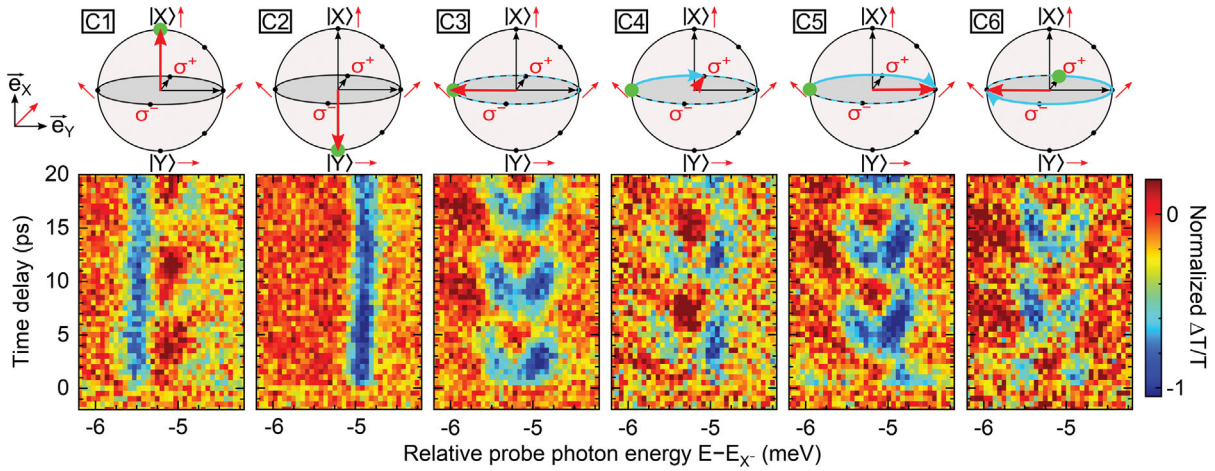

FIG. 3. Polarization control of quantum beats. Top: polarization configurations $C1$ to $C6$ visualized on Bloch spheres, representing superpositions of $|\mathrm{X}\rangle$ and $|\mathrm{Y}\rangle$. Points on the sphere are associated with probe polarizations (small red arrows and $\sigma^{+,-}$) relative to the axes $\vec{e}_\mathrm{X}$ and $\vec{e}_\mathrm{Y}$ (coordinate system at left). Green dots mark the excited superposition, thick red arrows the readout one. If a modulation exists ($C3$–$C6$), it is visualized in light blue (dashed line and arrow), rotating clockwise around the equator. Polarization configurations: $C1$ pump-probe linear along $\vec{e}_\mathrm{X}$; $C2$ pump-probe linear $\vec{e}_\mathrm{Y}$; $C3$ pump-probe linear $\vec{e}_\mathrm{X}-\vec{e}_\mathrm{Y}$; $C4$ pump linear $\vec{e}_\mathrm{X}-\vec{e}_\mathrm{Y}$, probe right-circular; $C5$ pump linear $\vec{e}_\mathrm{X}-\vec{e}_\mathrm{Y}$, probe linear $\vec{e}_\mathrm{X}+\vec{e}_\mathrm{Y}$; $C6$ pump left-circular, probe linear $\vec{e}_\mathrm{X}-\vec{e}_\mathrm{Y}$. Bottom: transient transmission for $C1$ to $C6$ color-coded versus time delay and probe photon energy relative to X^-.

(A) to (C), as shown in Fig. 2(d). The V-shaped forms (blue) and positive regions (dark orange) represent an excellent match to the experimental results in Fig. 2(e).

We now control the quantum beats by varying pump-probe polarizations. Six different configurations $C1$ to $C6$ are visualized in Bloch spheres at the top of Fig. 3, representing coherent superpositions of states $|\mathrm{X}\rangle$ and $|\mathrm{Y}\rangle$. Linear probe polarizations are visualized by thin red arrows. Their direction refers to the principal axes $\vec{e}_\mathrm{X}$ and $\vec{e}_\mathrm{Y}$ of the confinement potential, as exemplified by the coordinate system at left. Circular probe polarizations are marked by $\sigma^{+,-}$. Coherent superpositions initialized by the pump are indicated by green dots. Note that here, σ^+ and σ^- must be interchanged for pump and probe due to the selection rules for two-step resonant biexciton excitations. Each specific probe polarization is indicated by a thick red arrow pointing towards the readout state.

For $C1$ and $C2$, excitation and readout are set collinearly along $\vec{e}_\mathrm{X}$ or $\vec{e}_\mathrm{Y}$ to exclusively excite and probe $|\mathrm{X}\rangle$ or $|\mathrm{Y}\rangle$. The differential transmissions (Fig. 3) indeed show biexcitonic absorption solely at XX^-_X ($C1$) and at XX^-_Y ($C2$), respectively. No modulation occurs due to excitation of an eigenstate. In $C3$ to $C6$, coherent superpositions with identical contributions from $|\mathrm{X}\rangle$ and $|\mathrm{Y}\rangle$ are initialized. A collinear polarization along $\vec{e}_\mathrm{X}-\vec{e}_\mathrm{Y}$ is excited in $C3$, corresponding to the configuration discussed in Figs. 1 and 2. We now control the phase of the coherent beats by changing the probe polarization. $C4$ and $C5$ exhibit phase shifts of $\pi/2$ and π, respectively. Their origin is visualized by light blue arrows in the Bloch spheres: after initializing a specific superposition, the maximum amplitude is reached when it rotates in the equatorial plane until it phases up with the probe. Note that solely the relative polarization angle between pump and probe determines the temporal phase. This fact is demonstrated by $C6$ with a circular polarization used for pumping: a probe polarization identical to $C3$ shifts the phase by $3\pi/2$.

We can now understand why these signatures emerge so rapidly after excitation, despite the required relaxation from $|\mathrm{X}^*\rangle$ and $|\mathrm{Y}^*\rangle$ to $|\mathrm{X}\rangle$ and $|\mathrm{Y}\rangle$. Interestingly, only a broad resonance with a width of (3.4 ± 0.4) meV is discernible in a photoluminescence excitation (PLE) spectrum of the QD [21] where transitions from $|\mathrm{QDGS}\rangle$ into $|\mathrm{X}^*\rangle$ and $|\mathrm{Y}^*\rangle$ are located. Naively, one would expect two sharp resonances enabling the formation of a long-lived superposition state. These facts indicate an ultrafast relaxation of the P-shell hole into the S shell, providing both a rapid onset of biexcitonic absorption and a fast interband dephasing. For direct experimental access to the hole scattering, we measure with configuration $C2$ to isolate the dynamics leading from $|\mathrm{Y}^*\rangle$ to $|\mathrm{Y}\rangle$ [Fig. 4(a)]. Here, three transient absorptions emerge early after excitation with only one of them located at XX^-_Y (indicated by the blue arrow). Centered 6.1 meV below X^- (energy position marked with orange arrow), a second signature $\mathrm{XX}^-_\mathrm{YY}$ appears redshifted to both biexcitonic resonances. A third feature $\mathrm{XX}^-_\mathrm{YX}$ is slightly blueshifted to and partially overlaps with XX^-_Y. Its energetic position is centered 4.6 meV below X^- and marked with a green arrow. Note that as $\mathrm{XX}^-_\mathrm{YY}$, also feature $\mathrm{XX}^-_\mathrm{YX}$ is confined to short times t_D between 0 and 1 ps. We assign both lines to an induced absorption, establishing a hot biexciton including one P-shell hole: while residing in the photoexcited state $|\mathrm{Y}^*\rangle$ [Fig. 1(b)], absorbing a photon with an energy close to XX^-_Y forms a

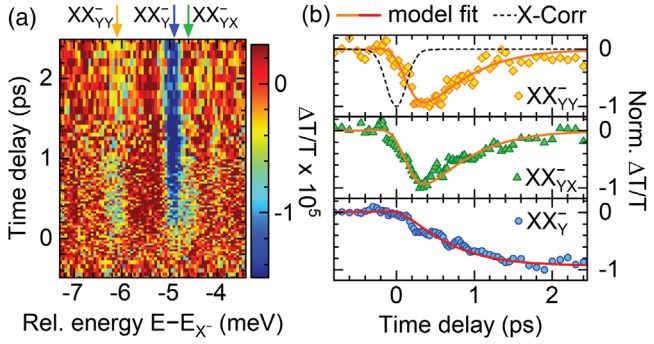

FIG. 4. Femtosecond relaxation of P-shell hole. (a) Color-coded differential probe transmission versus time delay and photon energy relative to X^-, as measured in configuration $C2$. (b) Spectral slices of normalized $\Delta T/T$ integrated over an energy interval of 0.4 meV centered around −6.1 (XX^-_{YY}), −4.9 (XX^-_{Y}), and −4.6 meV (XX^-_{YX}) versus time delay. Solid orange and red lines: least-square fits to theoretical model. Dashed black line: intensity cross-correlation between pump and probe.

hot biexciton. The minute shifts of XX^-_{YY} and XX^-_{YX} with respect to XX^-_{Y} result from slightly different Coulomb energies of the other involved carriers with respect to the P-shell hole. Spectral slices integrated over a 0.4-meV interval around XX^-_{YY} and XX^-_{YX} are depicted as yellow diamonds and green triangles in Fig. 4(b), respectively. The orange lines result from modeling the increase of induced absorption with the convolution of a nonresonant cross-correlation between pump and probe [dashed line at top of Fig. 4(b)] and an exponential decay related to a hole relaxation time τ_H of (390 ± 80) fs. As expected, the dynamics match for XX^-_{YY} and XX^-_{YX}. If the increase of absorption at XX^-_{Y} originates from relaxation of the P-shell hole, it should occur with the same time constant. Indeed, the time integral over the fitting functions at XX^-_{YY} and XX^-_{YX} [red graph at the bottom of Fig. 4(b)] agrees well with the blue circles extracted by spectrally slicing data from Fig. 4(a) around XX^-_{Y}. By PLE measurements, we determine the energy gap between valence-band S and D shells to (60 ± 10) meV [21]. Assuming parabolic confinement, a gap of (30 ± 5) meV between P and S shell results which is close to the longitudinal-optical phonon energy of CdSe of 25 meV [38]. This fact explains the femtosecond hole relaxation with a quasiresonant quantum kinetic coupling via the Fröhlich interaction [14,39].

In summary, we find a subnanosecond coherence time between hot-trion states in a single QD. Control over amplitude and phase of the resulting quantum beats in biexcitonic absorption is provided by the pump-probe polarizations. This option allows us to directly investigate the femtosecond relaxation of the P-shell hole. In contrast, trion spin coherence is protected from dephasing by identical orbital shell configurations of the states and limited solely by the energy relaxation of the p-shell electron requiring an electron-hole spin flip. This combination results in a difference between interband dephasing and trion coherence times by almost three orders of magnitude. The significant amount of fine-structure splitting between hot-trion states provides sub-THz frequencies for the evolution of coherent superpositions. We expect analogous phenomena to occur also in other species of zero-dimensional quantum systems whenever electron relaxation is slowed, e.g., by Pauli blocking and exchange splitting is large enough to provide adequate beat frequencies. These facts are rendering our observations relevant for the search of promising platforms for ultrafast quantum logic operations with extremely large processing bandwidth.

Funded by the Deutsche Forschungsgemeinschaft (DFG)—Project No. 425217212—SFB 1432.

*Present address: Department of Physics, Indian Institute of Technology Bombay, Mumbai, India.
†Alfred.Leitenstorfer@uni-konstanz.de

[1] D. P. DiVincenzo and D. Loss, J. Magn. Magn. Mater. **200**, 202 (1999).
[2] P. Michler, *Quantum Dots for Quantum Information Technologies* (Springer International Publishing, Cham, 2017).
[3] A. B. Henriques, A. Schwan, S. Varwig, A. D. B. Maia, A. A. Quivy, D. R. Yakovlev, and M. Bayer, Phys. Rev. B **86**, 115333 (2012).
[4] O. Gazzano, S. Michaelis de Vasconcellos, C. Arnold, A. Nowak, E. Galopin, I. Sagnes, L. Lanco, A. Lemaître, and P. Senellart, Nat. Commun. **4**, 1425 (2013).
[5] S. Sim, D. Lee, A. V. Trifonov, T. Kim, S. Cha, J. H. Sung, S. Cho, W. Shim, M.-H. Jo, and H. Choi, Nat. Commun. **9**, 351 (2018).
[6] J. Berezovsky, M. H. Mikkelsen, N. G. Stoltz, L. A. Coldren, and D. D. Awschalom, Science **320**, 349 (2008).
[7] G. Moody, R. Singh, H. Li, I. A. Akimov, M. Bayer, D. Reuter, A. D. Wieck, and S. T. Cundiff, Solid State Commun. **163**, 65 (2013).
[8] V. Giesz, N. Somaschi, G. Hornecker, T. Grange, B. Reznychenko, L. De Santis, J. Demory, C. Gomez, I. Sagnes, A. Lemaître, O. Krebs, N. D. Lanzillotti-Kimura, L. Lanco, A. Auffeves, and P. Senellart, Nat. Commun. **7**, 11986 (2016).
[9] D. Ding, M. H. Appel, A. Javadi, X. Zhou, M. C. Löbl, I. Söllner, R. Schott, C. Papon, T. Pregnolato, L. Midolo, A. D. Wieck, A. Ludwig, R. J. Warburton, T. Schröder, and P. Lodahl, Phys. Rev. Applied **11**, 031002 (2019).
[10] M. Geller, Appl. Phys. Rev. **6**, 031306 (2019).
[11] I. Schwartz, E. R. Schmidgall, L. Gantz, D. Cogan, E. Bordo, Y. Don, M. Zielinski, and D. Gershoni, Phys. Rev. X **5**, 011009 (2015).
[12] T. Suzuki, R. Singh, G. Moody, M. Aßmann, M. Bayer, A. Ludwig, A. D. Wieck, and S. T. Cundiff, Phys. Rev. B **98**, 195304 (2018).
[13] U. Woggon, *Optical Properties of Semiconductor Quantum Dots* (Springer, New York, 1997).
[14] C. Hinz, P. Gumbsheimer, C. Traum, M. Holtkemper, B. Bauer, J. Haase, S. Mahapatra, A. Frey, K. Brunner, D. E. Reiter, T. Kuhn, D. V. Seletskiy, and A. Leitenstorfer, Phys. Rev. B **97**, 045302 (2018).

[15] F. Sotier, T. Thomay, T. Hanke, J. Korger, S. Mahapatra, A. Frey, K. Brunner, R. Bratschitsch, and A. Leitenstorfer, Nat. Phys. **5**, 352 (2009).
[16] A. Greilich, S. E. Economou, S. Spatzek, D. R. Yakovlev, D. Reuter, A. D. Wieck, T. L. Reinecke, and M. Bayer, Nat. Phys. **5**, 262 (2009).
[17] D. Press, T. D. Ladd, B. Zhang, and Y. Yamamoto, Nature (London) **456**, 218 (2008).
[18] O. Zakharov, A. Rubio, X. Blase, M. L. Cohen, and S. G. Louie, Phys. Rev. B **50**, 10780 (1994).
[19] C. Traum, P. Henzler, S. Lohner, H. Becker, D. Nabben, P. Gumbsheimer, C. Hinz, J. F. Lippmann, S. Mahapatra, K. Brunner, D. V. Seletskiy, and A. Leitenstorfer, Rev. Sci. Instrum. **90**, 123003 (2019).
[20] S. Mahapatra, K. Brunner, and C. Bougerol, Appl. Phys. Lett. **91**, 153110 (2007).
[21] See Supplemental Material at http://link.aps.org/supplemental/10.1103/PhysRevLett.126.067402 for details concerning sample structures and stationary characterization, the dynamics of the fundamental trion resonance as well as derivations of spin configurations of trion triplet states and of Eq. (1). This text includes Refs. [22–27].
[22] C. Genet and T. W. Ebbesen, Nature (London) **445**, 39 (2007).
[23] P. W. Milonni and J. H. Eberly, *Laser Physics* (John Wiley & Sons, Inc., Hoboken, NJ, USA, 2010).
[24] I. A. Akimov, T. Flissikowski, A. Hundt, and F. Henneberger, Phys. Status Solidi **201**, 412 (2004).
[25] V. M. Axt, T. Kuhn, A. Vagov, and F. M. Peeters, Phys. Rev. B **72**, 125309 (2005).
[26] H.-P. Breuer and F. Petruccione, *The Theory of Open Quantum Systems* (Oxford University Press, New York, 2002).
[27] G. D. Mahan, *Many-Particle Physics* (Plenum Press, New York and London, 1981).
[28] I. A. Akimov, K. V. Kavokin, A. Hundt, and F. Henneberger, Phys. Rev. B **71**, 075326 (2005).
[29] M. Holtkemper, D. E. Reiter, and T. Kuhn, Phys. Rev. B **97**, 075308 (2018).
[30] J. Huneke, I. D'Amico, P. Machnikowski, T. Thomay, R. Bratschitsch, A. Leitenstorfer, and T. Kuhn, Phys. Rev. B **84**, 115320 (2011).
[31] M. E. Ware, E. A. Stinaff, D. Gammon, M. F. Doty, A. S. Bracker, D. Gershoni, V. L. Korenev, Ş. C. Bădescu, Y. Lyanda-Geller, and T. L. Reinecke, Phys. Rev. Lett. **95**, 177403 (2005).
[32] T. Guenther, C. Lienau, T. Elsaesser, M. Glanemann, V. M. Axt, T. Kuhn, S. Eshlaghi, and A. D. Wieck, Phys. Rev. Lett. **89**, 057401 (2002).
[33] F. Rossi and T. Kuhn, Rev. Mod. Phys. **74**, 895 (2002).
[34] D. E. Reiter, T. Kuhn, and V. M. Axt, Adv. Phys. X **4**, 1655478 (2019).
[35] S. Mukamel, *Principles of Nonlinear Optical Spectroscopy* (Oxford University Press, New York, 1995).
[36] D. E. Reiter, Phys. Rev. B **95**, 125308 (2017).
[37] D. E. Reiter, V. M. Axt, and T. Kuhn, Phys. Rev. B **87**, 115430 (2013).
[38] C. I. Contescu and K. Putyera, *Dekker Encyclopedia of Nanoscience and Nanotechnology* (CRC Press, Boca Raton, 2009).
[39] E. A. Zibik, T. Grange, B. A. Carpenter, N. E. Porter, R. Ferreira, G. Bastard, D. Stehr, S. Winnerl, M. Helm, H. Y. Liu, M. S. Skolnick, and L. R. Wilson, Nat. Mater. **8**, 803 (2009).

Correction: The formatting of the term labeled (A) in Eq. (1) of the PDF was inadvertently manipulated during the final production stage and has been fixed.